Acta Chemica Scandinavica, 1995: 49: 189–202
Printed in Belgium – all rights reserved

ACTA
CHEMICA SCANDINAVICA
ISSN 0904-213X

Computer Modeling of Interfaces Between Aqueous and Metallic Phases†

E. Spohr*

Department of Theoretical Chemistry, University of Ulm, Albert-Einstein-Allee 11, D-89069 Ulm, Germany

Spohr, E., 1995. Computer Modeling of Interfaces Between Aqueous and Metallic Phases. – Acta Chem. Scand. 49: 189–202 © Acta Chemica Scandinavica 1995.

The results of recent molecular dynamics simulations of pure water and aqueous solutions containing single ions in contact with metallic surfaces are reviewed. Water forms a densely packed, partially oriented layer of adsorbed molecules. The compact layer influences the adsorption of ions and atoms on the metal surface in the electrochemical environment. Free energies of adsorption have been calculated in order to investigate (i) specific adsorption of ions on metal surfaces in a series of calculations of fluoride, chloride and iodide adsorption near a model mercury surface and (ii) the thermodynamics of the charge-transfer reaction $I^- \rightarrow I^0 + e^-$ on Pt(100).

1 Introduction

Computer simulation methods pervade all fields of physical and chemical sciences in which questions are to be answered on the atomic level. Computer simulations are especially useful in statistical mechanics when it comes to the investigation of properties of liquids and solutions where the molecular nature of the solvent plays an important role. Modern electrochemistry now makes use of a number of methods that yield information about the interface on the molecular level; *in situ* scanning tunnel microscopy even provides real-space images of the interface (see, e.g. Ref. 1 and references therein). However, contrary to surface analysis in ultrahigh vacuum, it is usually not possible to image directly the main constituent of the interface, namely the solvent.

Simulation methods like molecular dynamics (MD) and Monte Carlo (MC) render possible the realistic modeling of the liquid phase near an electrochemical interface (e.g. Refs. 2–16) on the basis of the longstanding experience of classical computer simulations of electrolyte solutions. Ion transport to and from the electrode is an important elementary step of electrochemical reactions. In order to understand this step on the molecular level, the following properties of the interface should be understood among others, most desirably as a function of ion concentration, surface structure and applied external potential: (i) structure of the liquid phase in the interfacial region, (ii) polarization and microscopic electric fields, (iii) range of density inhomogeneities, (iv) size of the diffuse layer, (v) adsorption of ions in the inner or outer Helmholtz plane, (vi) structural changes of hydration complexes, (vii) (partial) charge transfer and (viii) currents of particles and charge.

In this work some of these questions are illuminated by means of examples taken from our recent work. In the following chapter the methods used and the interaction models that define the simulated system are briefly discussed. Next, the structure and polarization of pure water in the vicinity of the interface are investigated. Then, we take a look at the adsorption of halogenide ions on platinum and mercury surfaces. Finally, some thermodynamic aspects of charge transfer during electrode reactions using the example of I^-/I^0 near Pt(100) are discussed.

2 Models and methods

On the basis of microscopic interactions between particles, the classical equations of motion of atoms, ions and molecules are solved numerically. From the trajectories, averages over configurations are formed according to the methods of classical statistical mechanics.

Simulation times for the systems discussed below are typically in the range of several tens of picoseconds up to approximately one nanosecond. Typical systems consist of several hundred molecules and ions. Ionic concentrations in the interfacial region are often rather low. To model an electrochemical system on the molecular level, several hundred water molecules per ion need to be taken into account. Consequently, owing to computational limitations the number of ions in the simulation cell can only be very small at realistic concentrations. Therefore, the

† Invited lecture presented at the 8th Nordic Symposium on Computer Simulation of Liquids and Solids, June 15–17, 1994, Røros, Norway.

* To whom correspondence should be addressed.

simulations discussed below contain only one single ion dissolved in several hundred water molecules. The simulation temperature T is typically 300 ± 3 K, and most energy values are quoted in units of $kT_{300} = 2.5$ kJ mol^{-1} (k is Boltzmann's constant).

2.1 Interaction potentials. The forces acting between atoms, ions and molecules near the interface result, within the framework of the Born–Oppenheimer approximation, from a complex many-body interaction potential which includes, among others, polarization, induction and many-body dispersion forces and the properties of the delocalized electrons in the metal phase. Currently, this potential function cannot be calculated from first principles. Therefore, and because of limits in computer power, the *ansatz* is often made that the interactions are separable and pairwise additive. The pairwise additive interaction energies can either be derived from *ab initio* quantum chemical calculations or can be determined empirically in the form of 'effective' interaction potentials. The latter form usually incorporates many-body effects in a summary fashion. In spite of these limitations, pairwise additive forces offer a conceptual advantage: it is possible to understand and discuss the relationship between macroscopic or microscopic system properties and the interactions on the molecular level. Nevertheless, the effect of the approximations in the interparticle interactions on the results has to be assessed critically in every single case.

The interactions between two water molecules are described by the well known TIP4P model.[17] It is a rigid model without intramolecular degrees of freedom. The charge distribution and hence the electrostatic interactions are described by three point charges, two positive charges (0.52 elementary charges) on the hydrogen atoms and one negative charge on the symmetry axis of the molecule (shifted from the oxygen position by 0.15 Å towards the hydrogen atoms). The dipole moment of the model molecule is 2.177 D and thus larger than the gas-phase dipole moment of water (1.85 D). In this way the effect of the polarization of the water molecule in the liquid phase by many-body interactions is summarily accounted for. We are currently trying to describe the interface more realistically with a self-consistent treatment of polarization[18] through the implementation of polarizable models (e.g. Refs. 19–22). In addition to the electrostatic interactions, the short-range repulsion and the dispersion interactions between two molecules are described by a 12–6 Lennard-Jones term in the TIP4P model. The model is frequently applied to the description of properties of bulk liquid water and electrolyte solutions. It describes the 'open' water structure resulting from the formation of hydrogen bonds reasonably well.

The interactions between ions and water molecules are described by pairwise additive interactions between the ion and the hydrogen, oxygen and charge sites of the water molecule. They consist of Coulomb terms between the ion and the charges of the TIP4P model and a Lennard-Jones or exponential r^{-6} function to describe short-range and dispersion interactions. The hydration structure of F^-,[23] Cl^- [24] and I^- [25] ions is described reasonably well by these interaction potentials.

The non-electrostatic part of the water–metal interactions describes adsorption site, adsorption geometry and adsorption energy on the basis of pairwise additive interactions between the atoms of the water molecule and the lattice atoms of the metallic phase. It is derived from semiempirical calculations of the interactions between a platinum cluster and a water molecule[26] and from *ab initio* calculations of the interactions between a mercury cluster and a water molecule,[27] respectively. In addition to the non-electrostatic interactions, the response of the metal to the charge distribution in the liquid phase can be taken into account by introducing image interactions. It has been found that these surface-mediated interactions are only of minor importance for the properties of liquid water. They become important in ionic systems. In summary, the water–metal interactions describe largely the properties of the adsorbed water layer and the polarization of the interface. As an example, Fig. 1 shows the distance dependence of the water–platinum interaction for various adsorption sites (top) and various orientations (bottom).

There is little quantitative information about the strength of the interactions between ions and the metal surface. As we will point out below, this interaction needs to be known only *a posteriori* and not during the simulation. Therefore, simulation results can be combined with different model assumptions or model calculations, the reliability of which can in turn be assessed by the analysis. In the current work, we have analyzed both the simple image charge model where the ionic charge interacts with a continuum half-space with infinite dielectric constant. We also parametrized pairwise additive interaction potentials on the basis of *ab initio* calculations on the SCF niveau using effective core potentials for iodide–platinum[25] and halogenide–mercury clusters.[28] Figure 2 shows the quantum chemical interactions of Li^+ and I^- with the platinum surface and the image interaction of a monovalent ion with an ideal metal where the static image plane is located at $z = 0$.

The description of a complex chemical system by effective pairwise additive interaction potentials makes possible a simple interpretation of the properties of the electrochemical interface. However, this *ansatz* is a crude simplification because the influence of the electrons in the system is only an indirect one. Certainly, this is not adequate for electron-transfer processes. On the other hand, the properties of the system can be characterized by two diabatic potential surfaces (one for the charged and one for the uncharged state) in the limiting case of slow electron transfer; in the limiting case of fast electron transfer, ions can be described as species with a position-dependent effective charge. On the basis of these assumptions, the classical description of the interactions between atoms, ions and molecules is justified.

The results discussed below focus on the properties of

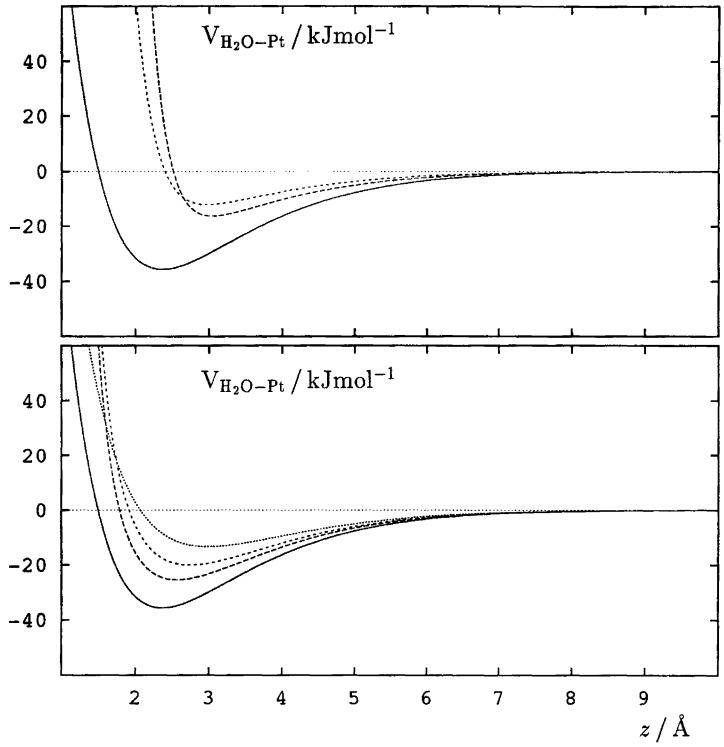

Fig. 1. Top: Total water–platinum(100) interaction energy as a function of the oxygen–surface distance z for water on top of a platinum atom (full line), on a bridge site (dashed), and on a four-fold hollow site (dotted). The dipole moment vector of the water molecule points away from the surface in all three cases. Bottom: Total water-platinum(100) interaction energy as a function of the oxygen–surface distance z for different orientations of water on top of a platinum atom: dipole vector pointing away from the surface (full line) and pointing towards the surface (dotted); dipole vector in the surface plane and proton–proton vector parallel to the surface (long-dashed) and perpendicular to the surface (short-dashed).

the aqueous phase. For the sake of the discussion, we will assume that the metal phase can be thought of reasonably well as some kind of external potential (either one-dimensional or through the collective effect of the atoms in a crystal) acting on the ions and molecules in the liquid phase.

2.2 Calculation of the free energy of adsorption. Because of the low number of ions in the simulation cell and the strongly inhomogeneous probability of finding the ions near the metal surface, it is currently hardly possible to directly simulate the density distribution function in a realistic system. The adsorption properties of the ion are more adequately described on the basis of the free excess energy or the potential of mean force (PMF).

The PMF $W(z)$ is related to the ionic density profile $\rho(z)$ in the following way:

$$\frac{W(z)}{kT} = -\ln\frac{\rho(z)}{\rho_{bulk}} = \frac{\Delta A^{exc}}{kT} \tag{1}$$

where k is Boltzmann's constant, T is the absolute temperature, z is the distance to the surface, ρ_{bulk} is the bulk ion density, and ΔA^{exc} is the excess free energy. The PMF of an ion or atom in the vicinity of the interface was calculated by the constraint molecular dynamics method due to Ciccotti *et al.*[29] In their method a constraint between two ions was introduced into the equations of motion. Here the method has been adapted by introducing a distance constraint between ion (atom) and the center of mass of the metal crystal. The solvent averaged mean force on the ion has been calculated by one MD simulation for each of various distances z' between ion and surface. The mean forces

$$\langle F_z\rangle(z') = \langle F_z^d\rangle(z') + \langle F_z^s\rangle(z') \tag{2}$$

are obtained as the sum of a direct contribution $\langle F_z^d\rangle(z')$ (calculated from the interactions between ion and metal) and a solvent contribution $\langle F_z^s\rangle(z')$. $\langle\ldots\rangle$ denote ensemble averages. The PMF $W(z)$ is obtained by integrating the mean force from a reference state (here the bulk solution, $z = -\infty$) up to a fixed distance z according to

$$W(z) = \int_{-\infty}^{z} \langle F_z\rangle(z')\mathrm{d}z' \tag{3}$$

$$= \int_{-\infty}^{z} \langle F_z^d\rangle(z')\mathrm{d}z' + \int_{-\infty}^{z} \langle F_z^s\rangle(z')\mathrm{d}z' \tag{4}$$

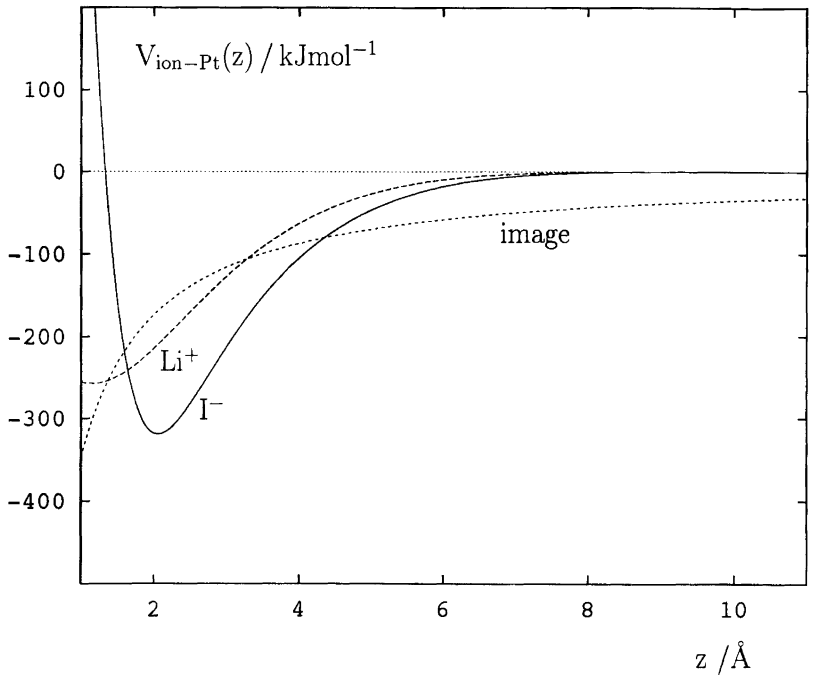

Fig. 2. Interaction energy of a Li^+ ion (dashed) and of an I^- ion (full) with the platinum (100) surface from the parametrized interaction potentials in Ref. 6. The dotted line shows the image interaction when the static image plane is located at $z=0$.

$$= W^d(z) \quad + W^s(z) \tag{5}$$

$W(z)$ is also the sum of the direct ion–metal contribution and the solvent contribution, which is caused by the thermal motion of the solvent molecules around the ion and near the interface. The contribution $W^s(z)$ must be calculated through a statistical mechanics simulation.

One remarkable property of this method is the fact that, within the framework of the pairwise additive approximation of interaction energies, the direct and the solvent contribution are decoupled. Therefore, the computationally expensive simulation of the solvent contribution can be combined with various models of the direct interactions between ion (atom) and metal. Below, ion adsorption is discussed both on the basis of the image charge model and on the basis of *ab initio* quantum chemical calculations.

3 Water structure near the metal surface

3.1 Absence of an external electric field. The structure of pure water near an interface is determined by the balance between hydrogen bond interactions and the adsorption energy. Figure 3 shows the oxygen density profile for a lamina of water that is confined on the left side by a smooth (9–3) Lennard-Jones surface that can be considered as a model for a free surface and on the right side by mercury with (111) surface structure. Owing to the significant adsorption energy of water on metal surfaces (typically of the order of 20–40 kJ mol^{-1}; see, e.g. Ref. 30) strong density oscillations are observed which are absent near the smooth wall. Figure 4 shows a snapshot from the simulation of a lamina consisting of 700 water molecules confined between 2 mercury surfaces on the left and right side. Ordered layers of adsorbed water molecules are clearly visible. Simulations of water near a Pt(100) surface show very similar results.[31]

The upper part of Fig. 5 shows the oxygen (full) and hydrogen (dashed) density profiles from the same simu-

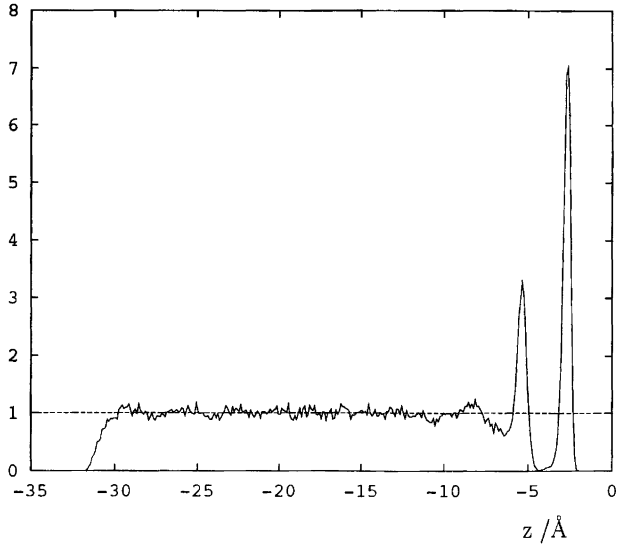

Fig. 3. Oxygen density profile from a 50 ps simulation of 385 water molecules that are confined on the left side by a simple (9–3). Lennard-Jones potential[49] and on the right side by mercury with (111) surface structure.

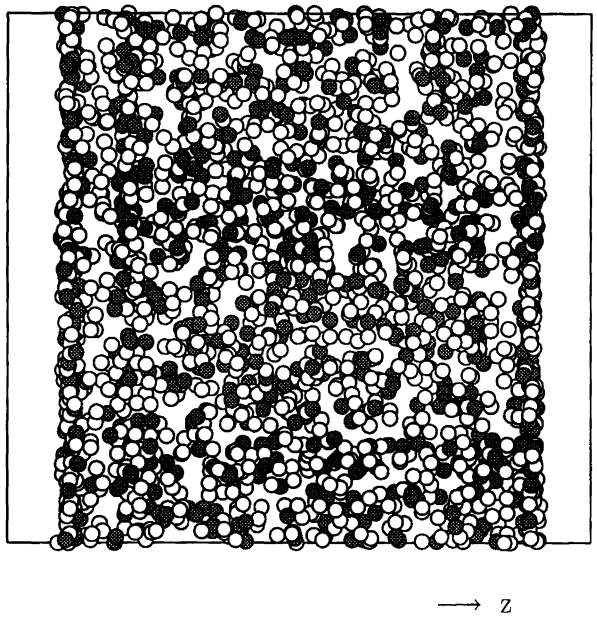

Fig. 4. Snapshot of a simulation of 700 water molecules between two model mercury surfaces with (111) surface structure. The mercury phases are located to the left and the right outside the frame. Oxygen atoms are shown as filled circles, hydrogen atoms as empty ones. The abscissa is the *z*-direction of the laboratory coordinate system. Periodic boundary conditions are applied along the other two directions. The ordered layers of adsorbed water molecules can be recognized easily together with the hydrogen atoms between first and second layers.

lation as in Fig. 4, averaged over 150 ps. The density is normalized to the bulk water density of 1000 kg m^{-3}. Clearly two layers are discernible in the oxygen profile; a third layer is just barely visible. The height of the first maximum is a direct measure for the adsorption energy of water (38 kJ mol^{-1} with the employed interaction potentials).[27] Integration of the density function from the surface to the minima near $\pm$ 10 Å yields the water coverage of 0.94 molecules per surface mercury. The second layer of water molecules is attached to the adsorbed layer by means of hydrogen-bonding interactions. This is evident from the pronounced interlayer maxima in the hydrogen profiles at about $\pm$ 10.5 and $\pm$ 9.6 Å which result from hydrogen bonds between hydrogen atoms of directly adsorbed molecules to the second layer and between hydrogen atoms of second layer molecules to the adsorbed layer, respectively (see also Ref. 32). The density in the center of the lamina is in very good approximation constant and equal to the bulk water density. (During the equilibration period, the position of the surfaces was adjusted to yield this density.) No oscillations persist throughout the lamina. Consequently, laminas of about 30 Å thickness can be used to simulate interfacial properties without significant coupling of the two interfaces. A more detailed analysis (see, e.g. Refs. 31 and 33) shows that the radial distribution functions and the diffusion coefficient are isotropic in the center of the lamina.

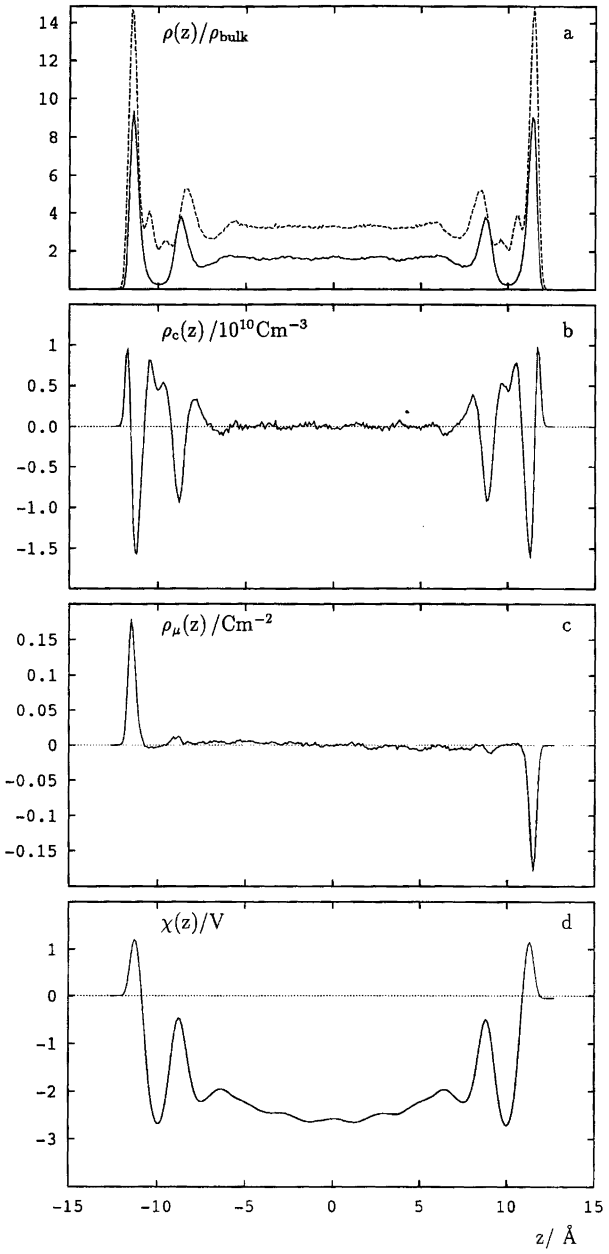

Fig. 5. (a) Oxygen (full) and hydrogen (dashed) density profiles. (b) Charge density ρ_c. (c) Dipole density ρ_μ. (d) Surface potential χ calculated from the charge density ρ_c by means of eqn. (6). All data are taken from a 150 ps simulation of 700 water molecules between two mercury phases with (111) surface structure.

From the atomic density profiles and the molecular orientations the charge density profile $\rho_c(z)$ and the dipole profile $\rho_\mu(z)$ can be calculated (Figs. 5b and 5c). For both the first and the second water layers, a quadrupolar charge profile (+ − +) is observed. The form of the charge profiles originates from the fact that mostly the center of mass (or the oxygen atoms) of the water molecules is localized, while the hydrogen density distribution is broadened due to librational motions and due to

the hydrogen bonding between layers. Beyond the second layers the charge density approaches zero within the limits of statistical uncertainty.

The dipole density profile $\rho_\mu(z)$ indicates ordered dipoles in the adsorbate layer. The orientation is largely due to the anisotropy of the water–metal interaction potential which favours configurations in which the oxygen atom is closer to the surface. Most quantum-chemical calculations of water near metal surfaces to date predict a significant preference of 'oxygen-down' configurations over 'H-down' ones at zero electric field.[26,27,33–36] The difference in sign on the left and right side of the lamina is a consequence of the vector nature of the dipole moment. The dipole orientation in the second layer is only weakly anisotropic. Furthermore, a weak orientational preference (positive values of ρ_μ in the left and negative values of ρ_μ in the right half of the lamina) persists throughout the lamina.

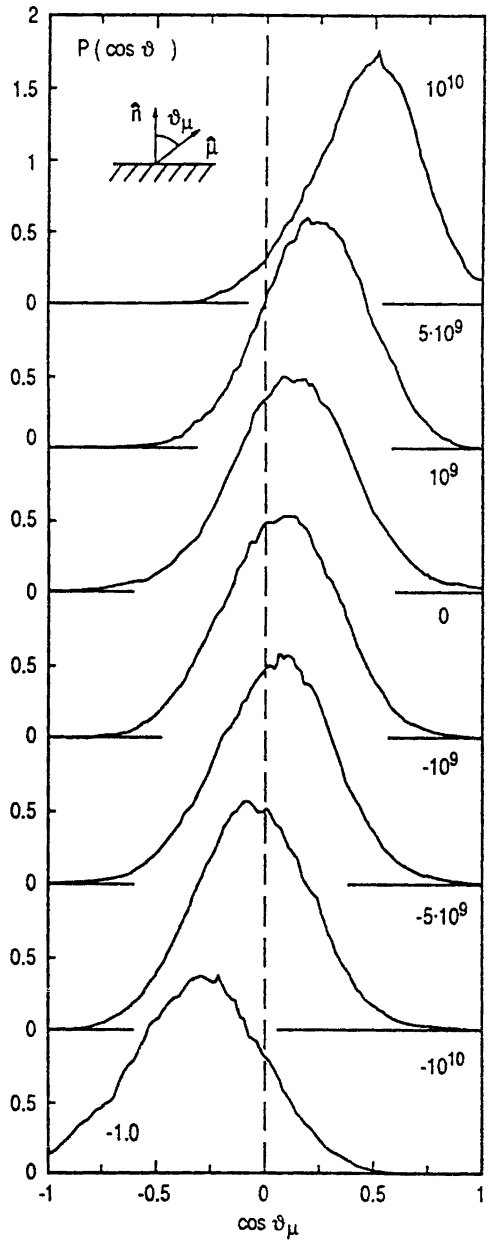

Fig. 6. Distribution of the cosine of the angle ϑ_μ between the dipole moment unit vector of the water molecule ($\hat{\mu}$) and the outward-directed surface normal ($\hat{z}$) for various homogeneous electric fields. The field strengths are given in units of V m^{-1}. Data are from simulations of 305 water molecules between Pt(100) surfaces.

Solving the one-dimensional Poisson equation with the charge density profile $\rho_c(z)$ leads to the electrostatic (dipolar) potential drop near the interface according to

$$\chi(z) = \int_{-\infty}^{z} q(z')(z - z')\mathrm{d}z' \qquad (6)$$

(see Fig. 5d). The potential drop across the first water layer is approximately 2.7 V. It is slightly reduced in the second layer and then slowly increases towards the final value $\chi(0) = 2.6$ V in the middle of the lamina. The slow increase of $\chi(z)$ in the central part of the lamina is related to the weak orientational preference visible in ρ_μ in that region. Experimentally, no value for χ has been determined yet free of assumptions. However, the most likely value of χ is around 0.2–0.3 V.[38] Hence, the results of the *ab initio* cluster calculates seem to crossly overestimate the orientational anisotropy of the water–metal interactions. On Pt(100), where water–metal interactions are based on semiempirical calculations, a smaller value of about 1.1 V was found.[31] We currently investigate the effect of the anisotropy of the water–metal interactions on the other properties of the interface by using a model water–surface potential in which we can systematically vary the anisotropy without varying other features like adsorption energy and corrugation.[39]

3.2 Interfacial water in an electric field. An external electric field changes the orientational distribution of water molecules in the interfacial region. Figure 6 shows the orientational distribution of the dipole moment vectors in the adsorbed water layer for various electrical surface charge densities (corresponding to homogeneous electric field according to $\rho = E\varepsilon_0$). The data are taken from simulations of 305 water molecules between two Pt(100) surfaces.[40] In the field-free case a wide orientational distribution with the first moment $\langle \cos \vartheta_\mu \rangle$ at approximately 0.1 is obtained. This corresponds to the observed dipole potential of roughly 1.1 V.[31] The preference of 'oxygen down' bonding is manifest in the large probability of positive values of cos ϑ (corresponding to angles smaller than 90° between dipole vector and surface normal). The tendency of water to form hydrogen bonds leads to the observed wide distribution, where most of the water dipoles are more or less oriented parallel to the surface. From the direct water–metal interaction potential, a narrow distribution around cos $\vartheta = 1$ would be expected.

For positive surface charges the moment of the distribution shifts towards larger absolute values and the distribution becomes slightly narrower. For low negative surface charge densities, the dipole orientational distribution becomes more symmetric around the parallel orientation. At larger negative surface charge densities, the orientational distribution changes in such a way that the hydrogen atoms point preferentially to the surface. Even at the highest surface charge densities of $\pm 8.4\ \mu C\ cm^{-2}$ the orientational distribution is still of similar width as in the field-free case. Complete ordering occurs only at unphysically large electric fields.

Recently, Melroy *et al.*[41] published the results of X-ray reflectivity measurements of dilute aqueous sodium fluoride solutions near positively and negatively charged silver electrodes with (111) surface geometry. Their analysis shows an oscillatory density profile with three or four density maxima near the interface, qualitatively similar to the results in Figs. 3 and 5. They also found a very large shift of the distance of the first maximum of the oxygen density profile from the electrode when going from positive to negative field strengths. The data could only be explained by an 'enormous'[41] increase in the water coverage to 1.1 and 1.8 water molecules per silver atom at negative and positive surface charge densities, respectively.

Figure 7 shows the oxygen density profile from MD simulations at various surface charge densities. As no quantum-chemical calculations for water adsorption on silver are currently available, the simulations were run for water near mercury with (111) surface structure. We do indeed observe a shift of the first maximum of the oxygen density in analogy to the results in Ref. 41. However, we do not observe any drastic increase in total particle density in the absorbed layer. Contrary to experiment, at the high field corresponding to surface charges of $\pm 17.7\ \mu C\ cm^{-2}$, the density decreases. However, as in the simulations by Watanabe *et al.*,[42–44] the liquid phase is unstable at this high field strength: there is a spontaneous transition to a ferroelectric crystalline phase. At all fields, the surface coverage is less than one water molecule per mercury atom. The surface spacing of mercury atoms is 3.2 Å, larger than the one for Ag(111) of 2.88 Å (neglecting surface reconstruction and relaxation). Therefore, the surface area of one silver atom on the Ag(111) surface is smaller by about 20% than in the simulation. Thus, a coverage of not larger than about 0.8 molecules per surface atoms would be expected from MD simulations. In spite of the simple or even simplistic nature of the interaction models used in the simulations, it seems very unlikely from the simulations and geometric considerations that water coverages as high as the ones quoted in Ref. 41 can occur. It may be speculated that the experimental results are an indication of specific adsorption or another yet unknown process on the electrode.

4 Free energy of adsorption of halogenide ions near a metal surface

Figure 8 summarizes the results obtained recently[15] for iodide adsorption near a platinum (100) surface. The line

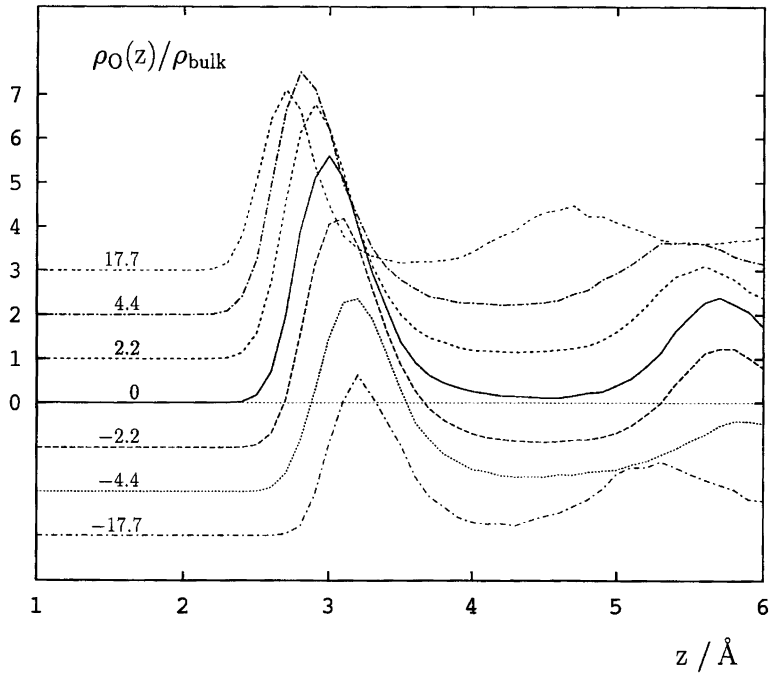

Fig. 7. Oxygen density profiles from 100 ps simulations of 700 water molecules between mercury surfaces with (111) surface structure in homogeneous external electric fields. The surface charge density (in units of $\mu C\ cm^{-2}$) is indicated.

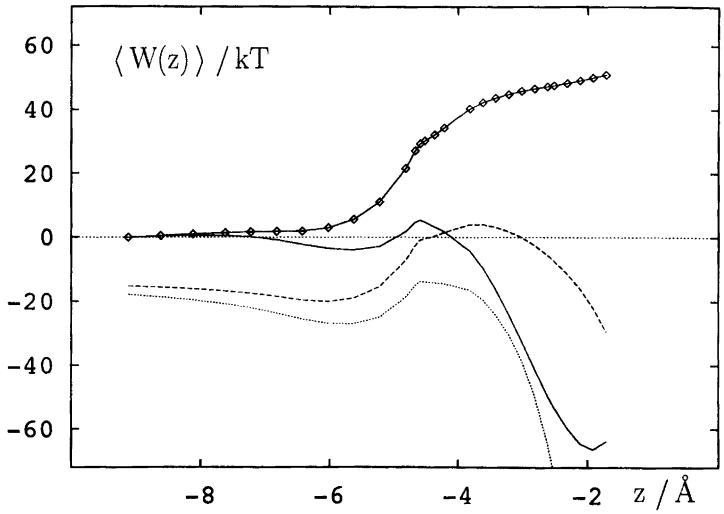

Fig. 8. The solvent contribution to the potential of mean force (diamonds) and the total potential of mean force between an iodide ion and a platinum surface on the basis of iodide–platinum interactions from *ab initio* calculations (full line). The remaining two curves are the combination of the solvent contribution with the image interaction of a monovalent ion with a metal surface where the image plane is located at $z=0$ Å (dashed) and $z=-1.39$ Å (dotted).

drawn through the diamonds shows the solvent contribution to the PMF as obtained by integration of the mean force. The sharp rise of the curve around -5 Å is the consequence of the displacement of adsorbed water molecules from the platinum surface once the iodide ion (radius in solution ≈ 2.2 Å) penetrates the adsorbed water layer (located at $z \approx -2.5$ Å)[31] and rearranges its hydration shell.

The remaining curves in Fig. 8 are the total (solvent + direct) PMFs calculated on the basis of different models for the ion–metal interaction potential. The combination of the solvent contribution to the PMF and the *ab initio* cluster potential[25] is given by the full line. The dashed and the dotted lines are obtained by assuming image charge interactions between the iodide ion and the metal surface. The image plane is located at $z = 0$ (dashed line) and at $z = -1.39$ Å (dotted line).

The PMF from the *ab initio* interaction potential describes the region close to the surface quite well. It exhibits a minimum at about 2 Å away from the surface corresponding to the direct adsorption of the ion. Further away from the surface, the *ab initio* potential energy decays too rapidly to model adequately the interactions with an extended polarizable metal surface.

On the other hand, the image potential energy curves describe the interaction of an ion in vacuum with a metal surface for large distances quite well but fail to reproduce a binding site on the surface. In the literature, there is some discussion about where the image plane is located relative to the top layer of surface atoms. The curves correspond to an image plane coinciding with the nuclei of the top layer of metal atoms ($z_I = 0$ Å, dashed line) and one that is shifted outwards into the solution by half the diameter of a platinum atom ($z_I = -1.39$ Å, dotted line). Preliminary *ab initio* investigations of the charge distribution in iodide–platinum clusters indicate that the image plane is located about 0.8 Å outside the top layer of platinum atoms.[45] Thus, the two curves using the image charge model for the iodide–platinum interactions can be regarded as extreme cases on either side of the realistic range of values. Estimates of the position of the static image plane based on the jellium model of the metal[46] support this view. Note that with the image interactions alone there is no possible stable contact-adsorption site for the ion, because the image potential approaches $-\infty$ for $z \rightarrow z_I$.

Independent of the exact shape of the direct iodide–metal interaction, all three PMFs clearly indicate the existence of an 'adsorption site' for a solvated ion at about $z = -5.5$ Å. There is a significant barrier (much higher than kT) between this state and the contact-adsorbed configuration in which the ion has partially lost its hydration shell. With all three direct interactions, the contact-adsorbed configuration is energetically lower than the configuration of the solvated ion. The relative energies of the two adsorption sites and the height and width of the barrier depend on the choice of the model for the direct iodide metal interactions.

An important issue in electrochemistry is the phenomenon of specific adsorption. An ion is considered to be adsorbed specifically in the 'inner Helmholtz plane' when it is partially dehydrated and in direct contact with the metal surface (see, e.g. Ref. 47). On the other hand, an ion that is adsorbed further away from the electrode with its hydration shell intact is considered to be adsorbed non-specifically in the 'outer Helmholtz plane'. In the classical treatment of contact adsorption, the balance between the energy of hydration of the ion and the strength of the image interactions determines which ions are specifically adsorbed and which ones are not.[47] We have in-

vestigated the problem by means of calculations of the free energy of adsorption (or, equivalently, the PMF for adsorption) of the halogenide ions F^-, Cl^- and I^- in 'infinitely dilute' aqueous solution (1 ion and 259 water molecules) near a mercury surface with (111) surface structure.[48]

Figure 9 shows as the primary result of these studies the solvent contribution to the PMF, W^s, of the three ions. The metal surface is located to the right. On the left side (at $z \approx -25$ Å) the lamina is confined by a smooth (9–3) Lennard-Jones surface analogous to that in Fig. 3.[49] At about 10–12 Å from both surfaces $W^s = 0$ within the limits of statistical uncertainty. This is equivalent to the fact that, on average, the forces on the hydrated ion are isotropic, and therefore the hydration shell is on average symmetric and bulk-like. Starting at about 6 Å from the surface, the solvent PMF W^s becomes repulsive for the iodide ion. This behaviour is in complete analogy to that observed on Pt(100) (see Fig. 8 and Ref. 15). The repulsion (e.g. $\approx 42\ kT$ at $z = -2$ Å) is slightly weaker than in the platinum case ($\approx 49\ kT$). The initial repulsive contribution to W^s originates from the work of hole formation on the surface. Because water molecules are adsorbed (or bound) on the surface, work needs to be done to desorb these water molecules before the ion can adsorb. With the applied water–mercury interaction potential[27] the binding energy of a water molecule on the surface is about 38 kJ mol^{-1} (or about 15 kT). Hence, removing three water molecules completely from the surface accounts for roughly 45 kT, which is the same order of magnitude as the observed value of 42 kT at contact. The 'steric' effect of removing the adsorbed water molecules shows up in the initial strong rise of the non-electrostatic contribution to W^s.[48] The water molecules are not completely removed from the surface, and the hole formation energy is not the only contribution to W^s. Hydration forces favour ion adsorption at larger distances. This is clearly shown by the dominance of electrostatic contributions to W^s at very small distances from the metal surface (see, e.g. Fig. 3 of Ref. 15).

Chloride (crosses in Fig. 9) shows a qualitatively similar behaviour as iodide. As the Cl^- ion is smaller than the I^- ion, the initial repulsion of the ion by solvent interaction is weaker than in the I^- case.

The behaviour of the fluoride ion (diamonds in Fig. 9) is qualitatively different from the larger ions. The solvent interactions stabilize the ion thermodynamically in the range from -8 to -5 Å, whereas the solvent effect is always repulsive for Cl^- and I^-. For F^-, obviously, the attraction by the adsorbed water layer (which is oriented preferentially with the hydrogen atoms pointing into the solution) dominates. The distance of the minimum (at about 5.5 Å) corresponds to an adsorbed species $F^-(H_2O)_6$ on top of the adsorbed layer of water molecules. A detailed analysis[48] shows that the very strong repulsion at distances below 5 Å is due to the hydration forces (indicated by the predominantly electrostatic nature of W^s in that region).

As above, we can apply different models of ion–metal interaction to calculate the total PMF. In Fig. 10 the solvent contribution W^s (diamonds) is shown together with the image interaction W^d (dashed) and the total PMF (crosses) for the F^- (top) and I^- (bottom) ions. The free-energy minimum for F^- is located around 5 Å from

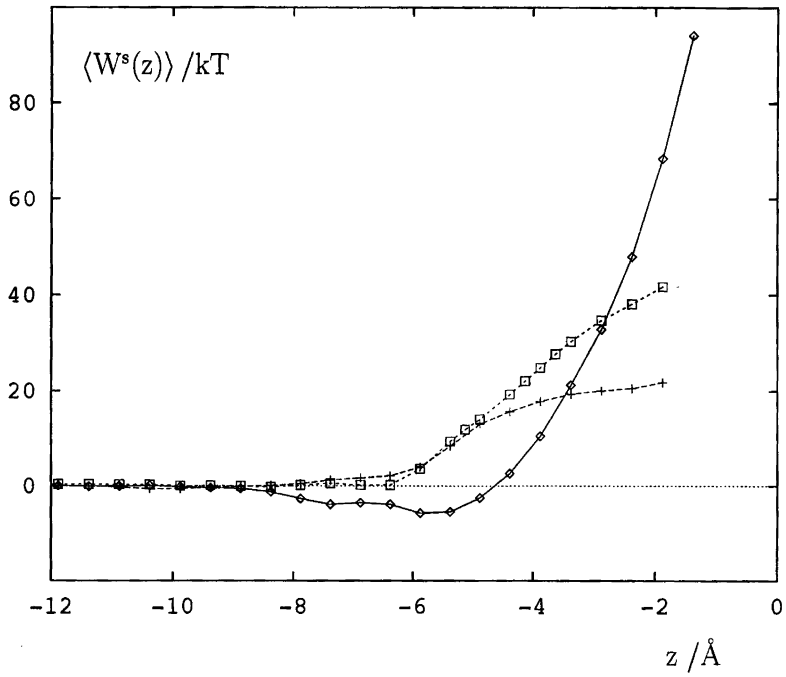

Fig. 9. The solvent contribution to the PMF of fluoride (diamonds), chloride (crosses) and iodide (squares) adsorbed near a mercury surface with (111) surface structure.

the surface. This is consistent with the picture of non-specific adsorption of the small, strongly hydrated anion.[47]

In the I^- case, there are, as in the case of adsorption on Pt(100),[15] two minima in the PMF. The lower one at $z = -2$ Å corresponds to the specifically adsorbed iodide state. The one around $z = -6$ Å corresponds to a weakly bound physisorbed state where the ion–hydration-shell complex is 'adsorbed' on top of the adsorbed water layer.

In Fig. 11 the solvent contribution W^s (diamonds) is shown together with the quantum-chemical interaction W^d (dashed) and the total PMF (crosses) for the F^- (top) and I^- (bottom) ions. The quantum-chemical cluster calculations of X^-–Hg_n clusters (X = F, Cl, I, n = 9,10,18) have been performed on the SCF level using basis sets of double-ζ quality.[28] The SCF energy data have been obtained for various distances above the on-top, bridge and hollow adsorption sites and have been fitted to an analytical function, similar to the case of water–metal interactions.[27,31] More details can be found in Ref. 28. The quantum-mechanical interaction is strongly attractive for both ions with an equilibrium ion–metal contact distance around 1.8 and 3.2 Å for F^- and I^-, respectively.

For the total PMF, only one minimum is found corresponding to specifically adsorbed ions. Owing to hydration, the equilibrium distances of both ions near the interface are shifted towards larger values as compared with the bare ion–metal interactions. The physisorbed region at distances of about 5–6 Å occurs only as a shoulder. Hence, the results of the quantum-chemical calculations do not seem to be in agreement with the 'conventional wisdom' in electrochemistry, where fluoride does not seem to be specifically adsorbed. There may be several explanations: First, the SCF calculations may not be adequate; electron correlation is certainly important. Therefore, calculations on a correlated level like MP2 and MP4 may be necessary. Second, the size of the mercury cluster may be too small to describe the metallic character of mercury properly. Third, many-body induction and dispersion effects (involving water molecules, ions and the metal cluster) are not accounted for. Clearly, this example shows that much more work needs to be done to understand the nature of the ion–metal interactions. Large-scale density functional calculations that have been recently performed [e.g. chloride overlayers on Ag(100)][50] are currently unable to generate a complete potential-energy surface for an isolated ion near the surface because of limitations in computer power and system size.

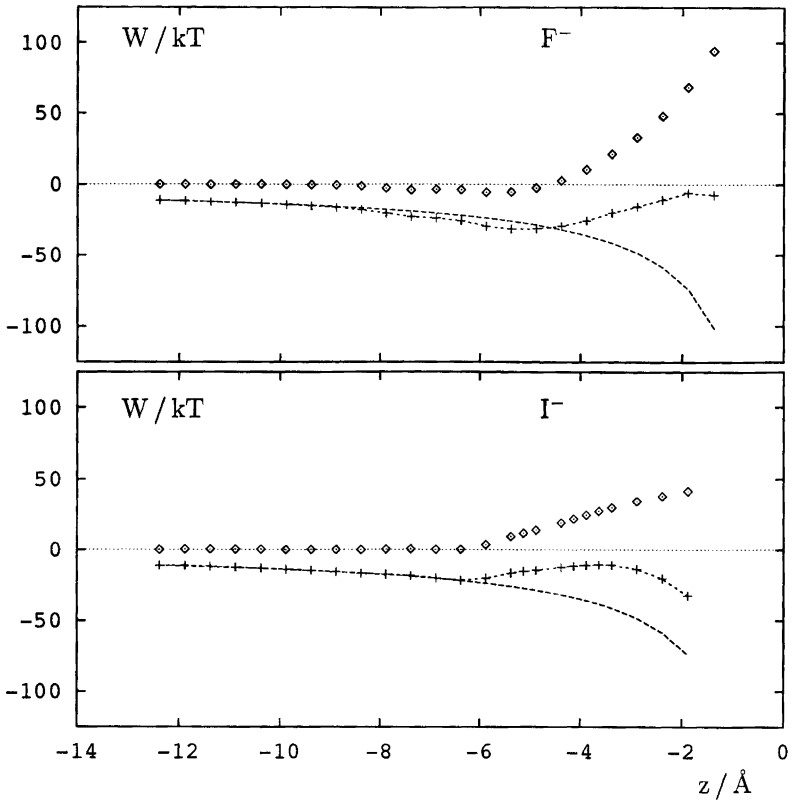

Fig. 10. Ion adsorption near mercury with (111) surface structure: solvent contribution to the PMF (diamonds), direct interactions (dashed) and total PMF (crosses) using the image charge model to describe ion–metal interactions. The position of the static image plane is at z=0. Top: fluoride, bottom: iodide.

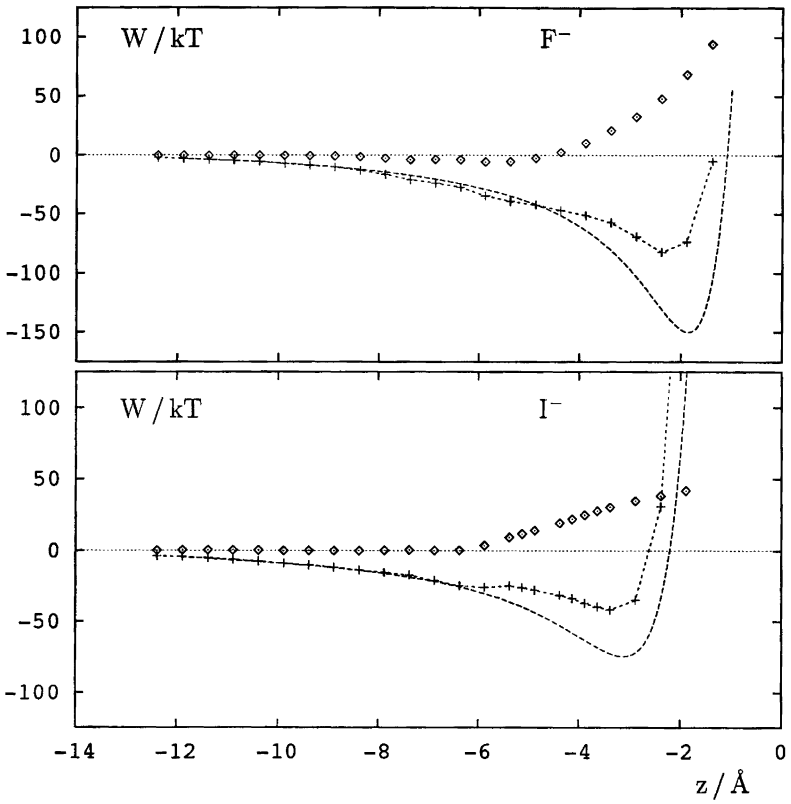

Fig. 11. Ion adsorption near mercury with (111) surface structure: Solvent contribution to the PMF (diamonds), direct interactions (dashed), and total PMF (crosses) using the quantum chemical ion–metal interaction potential. Top: fluoride, bottom: iodide.

5 Free energy of adsorption of the iodine atom and the iodide ion on a platinum surface

Recently we performed a study on the partial charge transfer of the I^- ion near the water–metal interface. The main results were: (i) the partial charge on the ion decreases rapidly with decreasing ion–metal distance, starting at around 5–6 Å from the surface, and (ii) ion hydration and the interaction with the dipolar field of the ordered adsorbed water layer stabilizes a larger partial charge on the ion in aqueous solution than in vacuum (see Ref. 16). Here, we want to present the essential results of a study of the diabatic free energy surfaces of I^0 and I^- in aqueous solution near the Pt(100) surface.[51]

The data for I^- have been taken from Ref. 15. The model of iodine is very simple: I^0 interacts with water by the non-electrostatic part of the I^-–water interactions.[25] Figure 12 shows the solvent contribution W^s to the PMF for the ion and the neutral atom. Like the case of the ion, the solvent PMF is purely repulsive for the atom. In the region from $z = -8$ Å to $z = -5$ Å both curves are almost identical. This is in keeping with the interpretation of this part of the free energy increase being due to 'steric' interactions rather than hydration forces (which are absent for the neutral I^0, as the hydration energy decreases almost to zero after removal of the electrostatic contribution to the interaction potential).

For distances smaller than about 4 Å from the surface, W^s decreases for the neutral atom. Once the atom has penetrated the compact surface layer and dislocated some of the adsorbed water molecules, the system stabilizes by pushing the atom towards the surface. The behaviour is an example for a hydrophobic effect where the 'insoluble' I^0 atom is pushed out of the aqueous phase. As it cannot be pushed into the solid metal phase, the contact-adsorbed geometry is the more favourable arrangement. The observed effect is entirely due to the I^0–water interactions.

In keeping the model simple, W^s has been combined with the *ab initio* interaction energy obtained for I^-–Pt_n clusters.[25] The image charge model has not been used here because additional assumptions would have to be made for the I^0–platinum interactions. The total PMFs of the iodine atom and the iodide ion are shown in Fig. 13. The total PMF is the excess free energy with respect to the bulk state. In order to compare the results, it is therefore necessary to take into account the differences in the solvation free energy G_{solv} (the solvation free energy of the iodide ion is much more negative than the free energy of solvation of the iodine atom) and the difference between the electron affinity E_a of the iodine atom and the Fermi energy E_f of the metal. The difference Δ between the two bulk levels is then given by

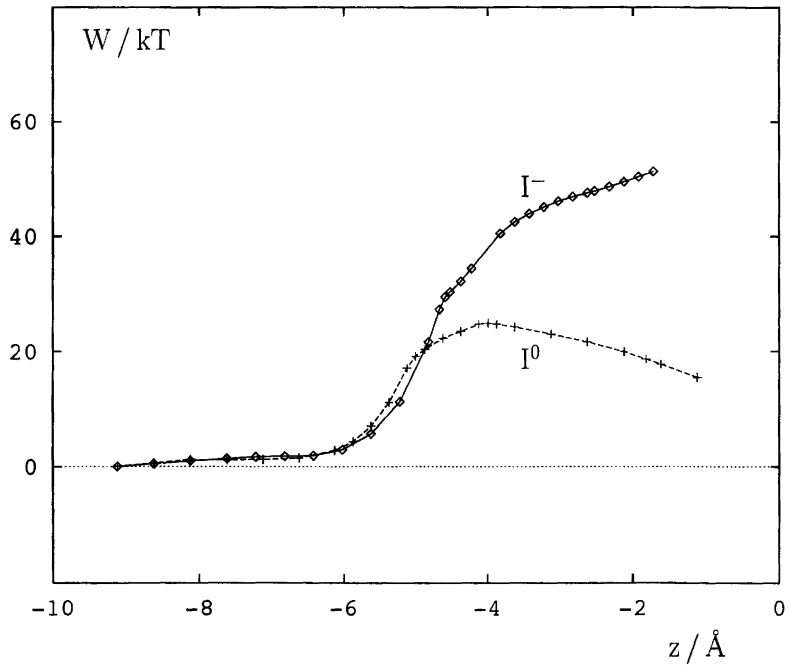

Fig. 12. Adsorption of iodide and iodine from aqueous solution on Pt(100): Solvent contribution to the PMF for I^- (diamonds) and I^0 (crosses).

$$\Delta = [G_{solv}(I^0) - G_{solv}(I^-)] + (E_a - E_f) = 19\,kT \qquad (7)$$

where the values of -296 kJ mol^{-1} [52] and 0 kJ mol^{-1} (from computer simulations)[53] have been used for $G_{solv}(I^-)$ and $G_{solv}(I^0)$, respectively, and values of 3.0591 and 5.65 eV for E_a and E_f, respectively.[54]

In both cases the free energy exhibits a minimum at a distance of about 2 Å from the surface, corresponding to specific adsorption of ion and atom. The solvent PMF (Fig. 12) favours the adsorption of iodine over iodide. While, naturally, the bulk level of I^- is lower than that of I^0, the surface level of I^0 is more stable than that of I^-.

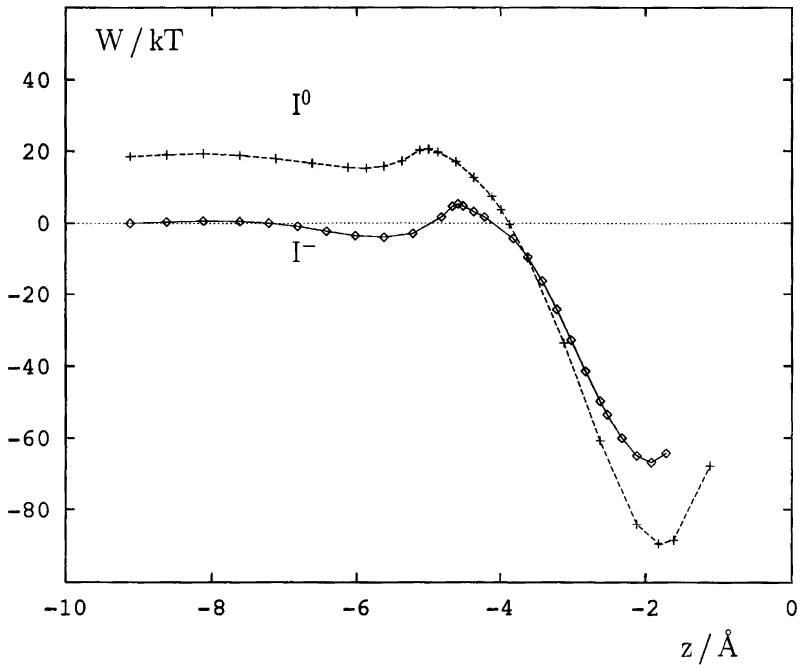

Fig. 13. Adsorption of iodide and iodine from aqueous solution on Pt(100): Total PMF for I^- (diamonds) and I^0 (crosses) on the basis of the quantum-chemical ion–metal interactions. The I^0 bulk level has been shifted by the amount Δ (see text).

Hence, the reaction $I^- \rightarrow I^0 + e^-$ is thermodynamically favourable near the Pt(100) surface.

6 Summary

Electrochemical problems can be investigated with simulation methods on the atomic level. We have first summarized the insight obtained from computer simulations of water–metal interfaces. Water forms a densely packed layer of adsorbed molecules on metal surfaces. Owing to the nature of the water–metal interactions the molecules are partially oriented and generate a potential drop across the interface. The adsorption of ions and atoms on metal surfaces from the aqueous phase is discussed on the basis of these structural features.

Adsorption of ions is observed both in the inner and in the outer Helmholtz plane. The results depend on the model for the ion–metal interactions. The simple image charge model describes qualitatively correctly the adsorption of fluoride in the outer Helmholtz plane and the specific adsorption of iodide on the surface. On the other hand, the more sophisticated quantum-chemical cluster calculations predict specific adsorption for all halogenide ions. The solvent influences the adsorption of ions near metal surfaces both 'sterically' (through the work that has to be done to remove adsorbed water from the surface) and electrostatistically (stabilisation of the fluoride ion in the outer Helmholtz plane). Experimentally, scanning tunnel microscopy of ordered iodine overlayers on platinum surfaces provides clear evidence for specific adsorption,[55,56] while fluoride ions are used in electrochemical experiments where specific anion adsorption is undesired.

The example of the adsorption of iodide and iodine on a Pt(100) surface demonstrates the possibility to calculate the free energy of adsorption, and, hence, the ability to predict the relative stability of charged and uncharged species near the surface. On the basis of a simple model that includes only hydration and adsorption of water on the surface, the charge transfer $I^- \rightarrow I^0 + e^-$ appears to be thermodynamically favourable.

Acknowledgements. Financial support by the *Fonds der Chemischen Industrie* and generous grants of computer time in the WAP workstation pool of the Department of Chemistry and by the Computer Center of the University of Ulm are gratefully acknowledged.

References

1. Kolb, D. M. In Lipkowski J. and Ross, P. N., Eds., *Structure of Electrified Interfaces*, p. 65, Verlag Chemie, Weinheim 1993.
2. Heinzinger, K. *Pure Appl. Chem. 63* (1991) 1733.
3. Raghavan, K., Foster, K., Motakabbir, K. and Berkowitz, M.L. *J. Chem. Phys. 94* (1991) 2110.
4. Halley, J. W., Pratt, S. and Johnson, B. *J. Electroanal. Chem. Interfacial Electrochem. 150* (1983) 355.
5. Rose D. A. and Benjamin, I. *J. Chem. Phys. 95* (1991) 6956.
6. Seitz-Beywl, J., Poxleitner, M. and Heinzinger, K. *Z. Naturforsch, Teil A 46* (1991) 876.
7. Glosli, J. N. and Philpott, M. R. *J. Chem. Phys. 96* (1992) 6962.
8. Rose, D. A. and Benjamin, I. *J. Chem. Phys. 98* (1993) 2283.
9. Glosli, J. N. and Philpott, M. R. In Halley, J. W. and Blum, L. Eds., *Microscopic Models Of Electrode-Electrolyte Interfaces*, Vol. 93-5, p. 90, Electrochemical Society, Inc., Princeton, NJ 1993.
10. Glosli, J. N. and Philpott, M. R. *J. Chem. Phys. 98* (1993) 9995.
11. Rose, D. A. and Benjamin, I. *J. Chem. Phys. 100* (1994) 3545.
12. Perera, L. and Berkowitz, M. L. *J. Phys. Chem. 97* (1993) 13803.
13. Xia, X. and Berkowitz, M. L. *Chem. Phys. Lett. 227* (1994) 561.
14. Straus, J. B. and Voth, G. A. *J. Phys. Chem. 97* (1993) 7388.
15. Spohr, E. *Chem. Phys. Lett. 207* (1993) 214.
16. Nazmutdinov, R. R. and Spohr, E. *J. Phys. Chem. 98* (1994) 5956.
17. Jorgensen, W. L., Chandrasekhar, J., Madura, J., Impey, R. W. and Klein, M. L. *J. Chem. Phys. 79* (1983) 926.
18. Kohlmeyer, A. Diplomarbeit, Universität Ulm, Ulm 1995.
19. Wallqvist, A. *Chem. Phys. Lett. 165* (1990) 437.
20. Zhu, S. B., Singh, S. and Robinson, G. W. *J. Chem. Phys. 95* (1991) 2791.
21. Rick, S. W., Stuart, S. J. and Berne, B. J. *J. Chem. Phys. 101* (1994) 6141.
22. Zhu, S. B., Yao, S., Zhu, J. B., Singh, S. and Robinson, G. W. *J. Phys. Chem. 95* (1991) 6211.
23. Nguyen, H. L. and Adelman, S. A. *J. Chem. Phys. 81* (1984) 4564.
24. Meier, W., Bopp, P., Probst, M. M., Spohr, E. and Lin, J.-L. *J. Phys. Chem. 94* (1990) 4672.
25. Seitz-Beywl, J., Poxleitner, M., Probst, M. M. and Heinzinger, K. *Int. J. Quant. Chem. 42* (1992) 1141.
26. Holloway, S. and Bennemann, K. H. *Surf. Sci. 101* (1980) 327.
27. Nazmutdinov, R. R., Probst, M. and Heinzinger, K. *J. Electroanal. Chem. 369* (1994) 227.
28. Toth, G., Spohr, E. and Heinzinger, K. *In preparation.*
29. Ciccotti, G., Ferrario, M., Hynes, J. T. and Kapral, R. *Chem. Phys. 129* (1989) 241.
30. Thiel, P. A. and Madey, T. E. *Surf. Sci. Rep. 7* (1987) 211.
31. Spohr, E. *J. Phys. Chem. 93* (1989) 6171.
32. Boecker, J., Nazmutdinov, R. R., Spohr, E. and Heinzinger, K. *Surf. Sci. In press.*
33. Spohr, E. *Chem. Phys. 141* (1990) 87.
34. Ribarsky, M. W., Luedtke, W. D. and Landman, U. *Phys. Rev. B 32* (1985) 1430.
35. Rosi, M. and Bauschlicher Jr., C. W. *J. Chem. Phys. 90* (1989) 7264.
36. Yang, H. and Whitten, J. L. *Surf. Sci. 223* (1989) 131.
37. Sellers, H. and Sudhakar, P. V. *J. Chem. Phys. 97* (1992) 6644.
38. Trasatti, S. *Personal communication.*
39. Spohr, E. *In preparation.*
40. Nagy, G., Heinzinger, K. and Spohr, E. *Faraday Discuss Chem. Soc. 94* (1992) 307.
41. Toney, M. F., Howard, J. N., Richter, J., Borges, G. L., Gordon, J. G., Melroy, O. R., Wiesler, D. G., Yee, D. and Sorensen, L. B. *Nature (London) 368* (1994) 444.
42. Watanabe, M., Brodsky, A. M. and Reinhardt, W. P. *J. Phys. Chem. 95* (1991) 4593.
43. Brodsky, A. M., Watanabe, M. and Reinhardt, W. P. *Electrochim. Acta 36* (1991) 1695.
44. Watanabe, M., Brodsky, A. M. and Reinhardt, W. P. *J. Chem. Phys. 95* (1991) 4593.

45. Nazmutdinov, R. *Personal communication.*
46. Lang, N. D. and Kohn, W. *Phys. Rev. B 7* (1973) 3541.
47. Bockris, J. O'M and Reddy, A. K. N. *Modern Electrochemistry*, Vol. 2, Plenum Press, New York 1977.
48. Eck, B. Diplomarbeit, Universität Ulm, Ulm 1994.
49. Lee, C. Y., McCammon, J. A. and Rossky, P. J. *J. Chem. Phys. 80* (1984) 4448.
50. Kramar, T., Podloucky, R. and Neckel, A. *Personal communication.*
51. Pecina, O., Spohr, E. and Schmickler, W. *J. Electroanal. Chem. Submitted.*
52. Atkins, P. W. *Physical Chemistry*, 4th Edn., Oxford University Press, Oxford 1990.
53. Spohr, E. *Unpublished results.*
54. Weast, R. C., Ed., *CRC Handbook of Chemistry and Physics*, 66th Edn., CRC Press, Boca Raton, FL 1987.
55. Vogel, R., Kamphausen, I. and Baltruschat, H. *Ber. Bunsenges. Phys. Chem. 96* (1992) 525.
56. Hubbard, A. T. *Chem. Rev. 99* (1988) 633.

Received October 31, 1994.